Inorg. Chem. **2006**, *45*, 10958–10966

Isostructural Bisdithiazolyl and Bisthiaselenazolyl Radicals: Trends in Bandwidth and Conductivity

Jaclyn L. Brusso,[1a] Shahab Derakhshan,[1a] Mikhail E. Itkis,[1b] Holger Kleinke,[1a] Robert C. Haddon,[1b] Richard T. Oakley,*[,1a] Robert W. Reed,[1a] John F. Richardson,[1c] Craig M. Robertson,[1a] and Laurence K. Thompson[1d]

Department of Chemistry, University of Waterloo, Waterloo, Ontario N2L 3G1, Canada, Department of Chemistry and Center for Nanoscale Science and Engineering, University of California, Riverside, California 92521-0403, Department of Chemistry, University of Louisville, Louisville, Kentucky 40292, and Department of Chemistry, Memorial University of Newfoundland, St. John's, Newfoundland A1B 3X7, Canada

Received September 6, 2006

Reaction of N-alkylated pyridine-bridged bisdithiazolylium cations [**1**]$^+$ (R_1 = Me, Et; R_2 = Ph) with selenium dioxide in acetic acid provides a one-step high-yield synthetic route to bisthiaselenazolylium cations [**2**]$^+$ (R_1 = Me, Et; R_2 = Ph). The corresponding radicals **1** and **2** can be prepared by chemical or electrochemical reduction of the cations. Structural analysis of the radicals has been achieved by a combination of single-crystal and powder X-ray diffraction methods. While the two sulfur radicals **1** adopt different space groups ($P3_121$ for R_1 = Me and $P\bar{1}$ for R_1 = Et), the two selenium radicals **2** (space groups $P3_121$ for R_1 = Me and $P3_221$ for R_1 = Et) are isostructural with each other and also with **1** (R_1 = Me, R_2 = Ph). Variable-temperature magnetic measurements on all four compounds confirm that they are undimerized $S = {}^1/_2$ systems, with varying degrees of weak intermolecular antiferromagnetic coupling. Variable-temperature electrical conductivity measurements on the two selenium radicals provide conductivities σ(300 K) = 7.4×10^{-6} (R_1 = Et) and 3.3×10^{-5} S cm^{-1} (R_1 = Me), with activation energies, E_{act}, of 0.32 (R_1 = Et) and 0.29 eV (R_1 = Me). The differences in conductivity within the isostructural series is interpreted in terms of their relative solid-state bandwidths, as estimated from Extended Hückel band-structure calculations.

Introduction

The concept of using neutral radicals as building blocks for single-component molecular conductors holds both appeal and challenge. In an ideal neutral radical conductor, the interactions between the singly occupied molecular orbitals (SOMOs) on an array of π-stacked radicals should give rise to a half-filled ($f = {}^1/_2$) energy band and a metallic ground state.[2] The radicals, however, must be fashioned so that in the solid-state, localized intermolecular bonding is minimized because such interactions lead to spin-quenching dimerization, that is, a Peierls distortion[3] and the opening of an energy gap at the Fermi level. At the same time, sufficient lattice-wide intermolecular interactions must be developed so that the electronic bandwidth W is sufficient to overcome the onsite Coulomb repulsion U which is a maximum for an $f = {}^1/_2$ system. If $W > U$, then a metallic state prevails, but if $W < U$, the system falls into a Mott insulating trap.[4]

In recent years, research into the development of neutral radical conductors has followed two slightly different paths.[5] The spiro-biphenalenyl systems pioneered by Haddon enjoy extremely low on-site Coulomb repulsion energies, by virtue of their zwitterionic formulation, and high room-temperature conductivities with $\sigma_{RT} \approx 10^{-1}$ S cm^{-1} have been achieved.[6] The conductivities nonetheless remain activated, indicating that the bandwidths W are not quite sufficient to eclipse U.

* To whom correspondence should be addressed. E-mail: oakley@uwaterloo.ca.

(1) (a) University of Waterloo. (b) University of California. (c) University of Louisville. (d) Memorial University.

(2) (a) Haddon, R. C. *Nature* **1975**, *256*, 394. (b) Haddon, R. C. *Aust. J. Chem.* **1975**, *28*, 2333. (c) Haddon, R. C. *Aust. J. Chem.* **1975**, *28*, 2343.

(3) Peierls, R. C. *Quantum Theory of Solids*; Oxford University Press: London, 1955; p 108.

(4) Mott, N. F. *Metal−Insulator Transitions*; Taylor and Francis: London, 1990.

(5) Rawson, J. M.; Alberola, A.; Walley, A. W. *J. Mater. Chem.* **2006**, *16*, 2560.

10.1021/ic061687c CCC: $33.50
Published on Web 12/06/2006

Chart 1

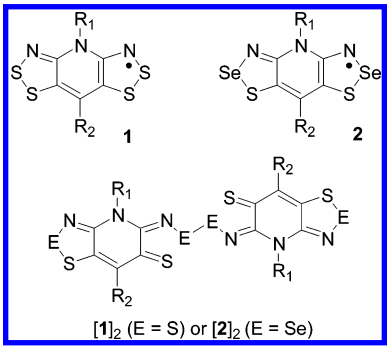

The other design model features heterocyclic thiazyl radicals and focuses more on the maximization of the bandwidth *W* while trying at the same time to maintain a low value for *U*.[7] Along these lines, we have recently explored the potential of resonance-stabilized bisdithiazolyl radicals **1** (Chart 1).[8,9,10] The extensive spin delocalization found in these compounds leads to low molecular disproportionation energies ΔH_{disp} and cell potentials E_{cell}, features which are critical for achieving a low value of *U* in the solid state.[11] However, while these materials display improved conductivities relative to monofunctional dithiazolyls, the thermal activation energies all lie in the range of $E_{act} = 0.4-0.5$ eV, indicating that the electronic bandwidth *W* is still far from sufficient to overcome the on-site Coulomb repulsion.

In an attempt to improve the performance of these resonance-stabilized radicals, we are exploring the effect of replacing sulfur by selenium on the structure and transport properties, a design approach recognized early on in the development of charge-transfer salts.[12] Recently, we described a lengthy stepwise method for the preparation of the mixed sulfur/selenium radicals, **2** (R_1 = Me, Et; R_2 = H).[13] To our surprise, these materials crystallized in the solid state not as radicals but rather as laterally Se−Se σ-bonded dimers, $[\mathbf{2}]_2$ (E = Se). These unusual dimers, which have also been observed for E = S,[14] behave as small band-gap semiconductors and show a remarkable response to applied pressure. Within the context of the neutral radical conductor paradigm, however, dimerization in this (or any other) mode sequesters charge carriers. To avoid this pitfall, we have sought to build radicals **2** with R_1 and R_2 selected to suppress association. Our first approach to this challenge has focused on the sulfur-based radical **1** (R_1 = Me, R_2 = Ph), the crystal structure (space group $P3_121$) of which is characterized (if not dictated) by the packing of the methyl and phenyl groups about the 3-fold screw axes. A similar arrangement is, of course, found for the dithiazolyl rings, which also form slipped π-stacked arrays clustered about the 3_1 axes. The question which we wished to answer was whether a sulfur/selenium replacement, that is, **1** → **2**, could be effected with retention of the space group. In other words, would it be possible to generate isostructural pairs of sulfur- and selenium-based radicals? If so, not only would we have achieved our goal of suppressing lateral dimerization, we would also have a unique opportunity to make a direct comparison of the effect of selenium-for-sulfur replacement on both bandwidth and conductivity. In this paper, we describe the preparation and structural characterization of two matched pairs of radicals **1** and **2** (R_1 = Me, Et; R_2 = Ph).[15] The results show that isostructural S → Se mapping is *sometimes* possible, that is, three of the four radicals **2** (R_1 = Me, Et; R_2 = Ph) and **1** (R_1 = Me; R_2 = Ph) have essentially the same crystal structures, belonging to the trigonal space group $P3_121$ (or $P3_221$). As such, the two selenium-based compounds represent the first Se-containing radicals that do *not* crystallize as dimers. Variable-temperature magnetic susceptibility and conductivity measurements have been performed on these radicals, and the results are interpreted in the light of Extended Hückel Theory (EHT) band calculations on the crystal structures.

Results and Discussion

Synthesis. We have recently shown that all three selenium-containing variants (SSeN, SeSN, and SeSeN) of monofunc-

(6) (a) Chi, X.; Itkis, M. E.; Patrick, B. O.; Barclay, T. M.; Reed, R. W.; Oakley, R. T.; Cordes, A. W.; Haddon, R. C. *J. Am. Chem. Soc.* **1999**, *121*, 10395. (b) Itkis, M. E.; Chi, X.; Cordes, A. W.; Haddon, R. C. *Science* **2002**, *296*, 1443. (c) Small, D.; Zaitsev, V.; Jung, Y.; Rosokha, S. V.; Head-Gordon, M.; Kochi, J. K. *J. Am. Chem. Soc.* **2004**, *126*, 13850. (d) Chi, X.; Itkis, M. E.; Kirschbaum, K.; Pinkerton, A. A.; Oakley, R. T.; Cordes, A. W.; Haddon, R. C. *J. Am. Chem. Soc.* **2001**, *123*, 4041. (e) Chi, X.; Itkis, M. E.; Reed, R. W.; Oakley, R. T.; Cordes, A. W.; Haddon, R. C. *J. Phys. Chem. B* **2002**, *106*, 8278. (f) Chi, X.; Itkis, M. E.; Tham, F. S.; Oakley, R. T.; Cordes, A. W.; Haddon, R. C. *Int. J. Quantum Chem.* **2003**, *95*, 853. (g) Pal, S. K.; Itkis, M. E.; Reed, R. W.; Oakley, R. T.; Cordes, A. W.; Tham, F. S.; Siegrist, T.; Haddon, R. C. *J. Am. Chem. Soc.* **2004**, *126*, 1478. (h) Liao, P.; Itkis, M. E.; Oakley, R. T.; Tham, F. S.; Haddon, R. C. *J. Am. Chem. Soc.* **2004**, *126*, 14297. (i) Mandal, S. K.; Itkis, M. E.; Chi, X.; Samanta, S.; Lidsky, D.; Reed, R. W.; Oakley, R. T.; Tham, F. S.; Haddon, R. C. *J. Am. Chem. Soc.* **2005**, *127*, 8185. (j) Pal, S. K.; Itkis, M. E.; Tham, F. S.; Reed, R. W.; Oakley, R. T.; Haddon, R. C. *Science* **2005**, *309*, 281. (k) Mandal, S. K.;. Samanta, S.; Itkis, M. E.; Jensen, D. W.; Reed, R. W.; Oakley, R. T.; Tham, F. S.; Donnadieu B.; Haddon, R. C. *J. Am. Chem. Soc.* **2006**, *127*, 1982.

(7) Cordes, A. W.; Haddon, R. C.; Oakley, R. T. *Phosphorus, Sulfur Silicon Relat. Elem.* **2004**, *179*, 673.

(8) Beer, L.; Brusso, J. L.; Cordes, A. W.; Haddon, R. C.; Itkis, M. E.; Kirschbaum, K.; MacGregor, D. S.; Oakley, R. T.; Pinkerton, A. A.; Reed, R. W. *J. Am. Chem. Soc.* **2002**, *124*, 9498.

(9) (a) Beer, L.; Brusso, L. J.; Cordes, A. W.; Haddon, R. C.; Godde, E.; Itkis, M. E.; Oakley, R. T.; Reed, R. W. *Chem. Commun.* **2002**, 2562. (b) Beer, L.; Britten, J. F.; Brusso, J. L.; Cordes, A. W.; Haddon, R. C.; Itkis, M. E.; MacGregor, D. S.; Oakley, R. T.; Reed, R. W.; Robertson, C. M. *J. Am. Chem. Soc.* **2003**, *125*, 14394.

(10) Beer, L.; Britten, J. F.; Clements, O. P.; Haddon, R. C.; Itkis, M. E.; Matkovich, K. M.; Oakley, R. T.; Reed, R. W. *Chem. Mater.* **2004**, *16*, 1564.

(11) ΔH_{disp} is the enthalpy change for the conversion of two gas-phase radicals, R, into a cation/anion pair (i.e., $2R \rightleftharpoons R^+ + R^-$) and is equal to the difference between the ionization potential (IP) and electron affinity (EA). The cell potential, $E_{cell} = E_{1/2}(ox) - E_{1/2}(red)$, is the difference between the half-wave potentials for the oxidation and reduction processes.

(12) (a) Beechgaard, K.; Cowan, D. O.; Bloch, A. N. *J. Chem. Soc., Chem. Commun.* **1974**, 937. (b) Engler, E. M.; Patel, V. V. *J. Am. Chem. Soc.* **1974**, *96*, 7376. (c) Bendikov, M.; Wudl, F.; Perepichka, D. F. *Chem. Rev.* **2004**, *104*, 4891.

(13) (a) Beer, L.; Brusso, J. L.; Haddon, R. C.; Itkis, M. E.; Leitch, A. A.; Oakley, R. T.; Reed, R. W.; Richardson, J. F. *Chem. Commun.* **2005**, 1543. (b) Beer, L.; Brusso, J. L.; Haddon, R. C.; Itkis, M. E.; Kleinke, H.; Leitch, A. A.; Oakley, R. T.; Reed, R. W.; Richardson, J. F.; Secco, R. A.; Yu, X. *J. Am. Chem. Soc.* **2005**, *127*, 1815.

(14) Leitch, A. A.; McKenzie, C. E.; Oakley, R. T.; Reed, R. W.; Richardson, J. F.; Sawyer, L. D. *Chem. Commun.* **2006**, 1088.

(15) For a preliminary communication of part of this work, see: Beer, L.; Brusso, J. L.; Haddon, R. C.; Itkis, M. E.; Oakley, R. T.; Reed, R. W.; Richardson, J. F.; Secco, R. A.; Yu, X. *Chem. Commun.* **2005**, 5745.

tional 1,2,3-dithiazolylium cations can be prepared by ring-closure reactions of S- and Se-acylated aminothiols and aminoselenols with sulfur and selenium oxyhalides.[16] This methodology can also be extended to the elaboration of mixed bifunctional derivatives, that is, salts of the bisthiaselenazolylium cations [**2**]$^+$ (R_1 = Me, Et; R_2 = H), but the synthetic sequence is lengthy. In the pursuit of a simpler and more general preparative route to these latter derivatives, we considered the direct insertion of selenium into the preformed bisdithiazolylium cation [**1**]$^+$. This idea was based on the early report[17] that monofunctional benzo-1,2,3-dithiazolylium salts could be converted regiospecifically into benzo-1,2,3-thiaselenazolylium salts by treatment with selenium dioxide in refluxing acetic acid.[18] To our satisfaction, we found that this method also works for our bifunctional materials.[15] Thus, the selenium-containing salts [**2**][OTf] (R_1 = Me, Et; R_2 = H; OTf^- = trifluoromethanesulfonate), previously prepared by the lengthy ring-closure method, could be made in *one step* starting from the readily prepared sulfur compounds [**1**][OTf]. Progress of the reaction was conveniently monitored by ESI mass spectrometry, which established the extent of selenium incorporation. While small amounts of material corresponding to the introduction of one and three selenium atoms were observed, the reaction essentially halted after the insertion of two seleniums, that is, with the formation of two SSeN rings, as in [**2**]$^+$. Attempts to force complete replacement of the remaining sulfurs by selenium by prolonged heating in HOAc in the presence of excess SeO_2, simply led to degradation of the heterocyclic framework. Recrystallization of the crude products from MeCN eliminated the trace quantities of one- and three-selenium containing materials and afforded pure [**2**][OTf].

The selenium insertion reaction proceeds smoothly with other substituents. Thus [**1**][OTf] (R_1 = Me, Et; R_2 = Ph), prepared from 2,6-dichloro-4-phenylpyridine **3** by the sequence shown in Scheme 1,[10] was readily converted into [**2**]-[OTf] (R_1 = Me, Et; R_2 = Ph). Bulk samples of the radicals **1** and **2** (R_1 = Me, Et; R_2 = Ph) were then generated by reduction of these salts with decamethylferrocene (DMFc) in MeCN. Needles of the sulfur radicals **1** (R_1 = Me, Et; R_2 = Ph) suitable for single-crystal X-ray work were prepared using H-cell techniques, that is, the slow diffusion of a solution of [**1**][OTf] (R_1 = Me, Et; R_2 = Ph) in MeCN into a solution of DMFc in MeCN. H-Cell methods, this time using octamethylferrocene (OMFc) as reducing agent, also afforded needles of **2** (R_1 = Et, R_2 = Ph) of sufficient size for single-crystal X-ray work. For **2** (R_1 = Me, R_2 = Ph), we were unable to generate crystals large enough for single-crystal analysis. We were, however, able to determine the structure of this material using powder X-ray diffraction and Rietveld refinement methods (vide infra).

Scheme 1

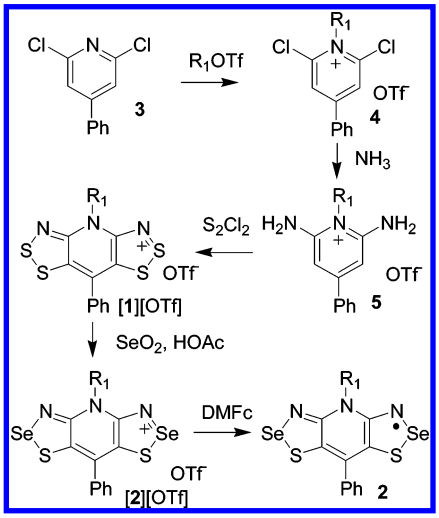

Table 1. Electrochemical,[a] EPR,[b] Magnetic, and Conductivity Data

compound[c]	**1** (R_1 = Et)	**1** (R_1 = Me)	**2** (R_1 = Et)	**2** (R_1 = Me)
$E_{1/2}^{(+1/+2)}$	1.295	1.305	1.245	1.255
$E_{1/2}^{(0/+1)}$	−0.118	−0.104	−0.097	−0.082
$E_{1/2}^{(-1/0)}$	−0.970	−0.956	−0.874	−0.850
E_{cell}	0.852	0.852	0.777	0.768
g	2.0086	2.0086	2.0113	2.0114
a_N (2 N)	0.317	0.32	0.32	0.32
a_N (1 N)	0.06	0.06	0.06	0.06
a_H	0.02	−	0.02	−
χ_D[d]	−181.13	−172.2	−197.13	−188.2
C[e]	0.334	0.475	0.349	0.491
Θ (K)	−0.9	−177	−19.5	−65.3
σ(300 K)[f]	$<10^{-7}$	$\sim10^{-7}$	7.4×10^{-6}	3.3×10^{-5}
E_{act} (eV)	−	−	0.32	0.29

[a] $E_{1/2}$ values (V) in MeCN, ref SCE; $E_{cell} = E_{1/2}^{(0/+1)} - E_{1/2}^{(-1/0)}$. [b] Coupling constants a_N and a_H in mT. [c] R_2 = Ph for both **1** and **2**. [d] χ_D in emu mol^{-1}. [e] C in emu K mol^{-1}. [f] σ(300 K) in S cm^{-1}.

Electrochemistry and EPR Spectroscopy. The design of neutral radical conductors requires the development of materials with low onsite Coulomb repulsion energies U. While the value of U is not easily predicted, it is well-established that trends in the gas-phase disproportionation enthalpies ΔH_{disp} for a series of related radicals provide a working mirror to the subsequent trends in U.[19] To this extent, the development of the resonance-stabilized framework of **1** represented a major improvement because both its ΔH_{disp} and E_{cell} values were markedly reduced relative to those of previously studied materials.[8,9] Model (B3LYP/6-31G**) calculations on **2** (R_1 = R_2 = H) suggest that the incorporation of selenium into the bisdithiazolyl framework further lowers the value of ΔH_{disp}.[13] Cyclic voltammetry experiments on the series of compounds [**1**][OTf] and [**2**]-[OTf] (R_1 = Me, Et; R_2 = Ph) confirm these predictions. The results, presented in the form of half-wave potentials $E_{1/2}$, are summarized in Table 1. In the case of the previously characterized sulfur-based radicals **1**, a series of waves corresponding to the −1/0, 0/+1, and +1/+2 redox couples were observed. The two more-anodic processes were always

(16) Oakley, R. T.; Reed, R. W.; Robertson, C. M.; Richardson, J. F. *Inorg. Chem.* **2005**, *44*, 1837.
(17) Akulin, Y. I.; Gel'mont, M. M.; Strelets, B. Kh.; Efros, L. S. *Khim. Geterotsikl. Soedin*. **1978**, 912.
(18) A similar approach has been used to incorporate selenium into 1,2,3,5-dithiazolylium salts. For example, see: Less R. J.; Rawson, J. M.; Jones, M. *Polyhedron* **2001**, *20*, 523.
(19) (a) Kaszynski, P. *J. Phys. Chem. A* **2001**, *105*, 7626. (b) Boeré, R. T.; Roemmele, T. L. *Coord. Chem. Rev.* **2000**, *210*, 369. (c) Kaszynski, P. *J. Phys. Chem. A* **2001**, *105*, 7615.

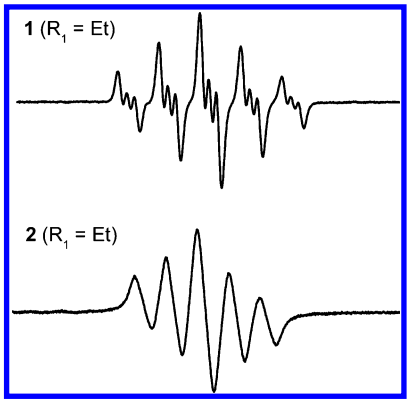

Figure 1. EPR spectra of **1** and **2** (R_1 = Et, R_2 = Ph) in DCM: SW = 0.4 mT.

reversible, but the reversibility of the −1/0 process required the presence of electron-accepting R_2 substituents. This we attributed to the fragility of the S−S[20] (or S−N)[21] bond in the reduced state. Similar problems were encountered with the first examples of bisthiaselenazolyls **2** (R_1 = Me, Et; R_2 = H), but this was further exacerbated by the insolubility of these materials resulting from their tendency to dimerize and precipitate out of solution. Some solubility issues were encountered with **2** (R_1 = Me, Et; R_2 = Ph); however, they were not nearly as severe as those seen earlier. Indeed, we have been able to obtain reversible waves for all three redox couples of both **1** and **2** (R_1 = Me, Et; R_2 = Ph). As may be seen in Table 1, the incorporation of selenium has the desired effect of reducing the resulting cell potentials E_{cell} by ∼70 mV; therefore, a lower onsite Coulomb potential, *U*, should follow.

The extent of spin delocalization in the sulfur- and selenium-based radicals **1** and **2** (R_1 = Me, Et; R_2 = Ph) has been probed by EPR spectroscopy. Representative EPR spectra, that is, those of **1** and **2** (R_1 = Et), recorded on samples dissolved in dichloromethane (DCM) at room temperature, are shown in Figure 1. The *g* values and ^{14}N and ^{1}H hyperfine coupling constants derived by simulation are listed in Table 1. As may be seen, the spectra are characterized by a five-line pattern resulting from spin coupling to the two equivalent ^{14}N nuclei on the two dithiazolyl (or thiaselenazolyl) rings. Smaller coupling to the pyridine nitrogen was extracted by spectral simulation. As expected, the spectra of the selenium-based radicals are broadened by spin−orbit effects, but otherwise, the similarity in the coupling constants for **1** and **2** suggest very similar spin distributions, as predicted by theoretical calculations.[13b]

Crystal Structures. We have structurally characterized all four radicals, **1** and **2** (R_1 = Me, Et; R_2 = Ph), by X-ray crystallography. Earlier analyses of **1** (R_1 = Me, R_2 = Ph)[10] and **2** (R_1 = Et, R_2 = Ph)[15] established that the two compounds were essentially isostructural, their trigonal space groups, $P3_121$ and $P3_221$, differing only in the sense of their chirality; crystal data are listed in Table 2. While we were unable to grow crystals of **2** (R_1 = Me, R_2 = Ph) of sufficient size for single-crystal X-ray work, powder diffraction measurements on this material have now allowed us to establish that its structure is closely related to that of the first two structures. The powder X-ray data (Figure 2) were analyzed using Rietveld methods, starting from the coordinates and space group of **1** (R_1 = Me, R_2 = Ph), and allowed for isotropic refinement of all non-hydrogen atoms excluding the peripheral carbons. Crystal data are provided in Table 2, and two views of the structure are shown in Figures 3 and 4. All intramolecular distances are nominal; a summary of pertinent intermolecular contacts is presented in Table 3.

The appearance of the unit cell of **2** (R_1 = Me, R_2 = Ph) (Figure 3) is virtually identical to that previously observed for **2** (R_1 = Et, R_2 = Ph) and **1** (R_1 = Me, R_2 = Ph).[10,15] Most notable, at the molecular level, is the fact that neither of the selenium-based radicals are dimerized. This is in stark contrast to all previously characterized selenazyl radicals, which associate either through cofacial overlap of their

Table 2. Crystallographic Data

	1[a]		**2**[a]	
	(R_1 = Et)	(R_1 = Me)	(R_1 = Et)	(R_1 = Me)
a (Å)	10.327(2)	16.182(3)	15.733(6)	15.6723(8)
b (Å)	15.407(4)	–	–	–
c (Å)	19.409(4)	4.2947(12)	4.973(3)	4.6889(7)
α (deg)	85.129(4)	–	–	–
β (deg)	75.059(4)	–	–	–
γ (deg)	70.421(4)	–	–	–
V (Å^3)	2811.3(11)	974.0(4)	1066.0(9)	997.4(1)
ρ_{calcd} (g cm^{-1})	1.590	1.649	2.011	2.094
space group	$P\bar{1}$	$P3_121$	$P3_221$	$P3_121$
Z	8	3	3	3
temp (K)	298(2)	293(2)	298(2)	293(2)
μ (mm^{-1})	0.667	0.718	5.487	-
λ (Å)	0.71073	0.71073	0.71073	1.54056
data/restraints/params	7824/0/723	1500/0/99	1401/12/106	
solution method	direct methods	direct methods	direct methods	powder data[b]
R, R_w (on F^2)	0.0615, 0.1456	0.0363, 0.0725	0.0605, 0.1242	0.0573, 0.0779[c]

[a] R_2 = Ph for both **1** and **2**. [b] Starting model taken from **1** (R_1 = Me). [c] R_p and wR_p, respectively, from the Rietveld refinement.

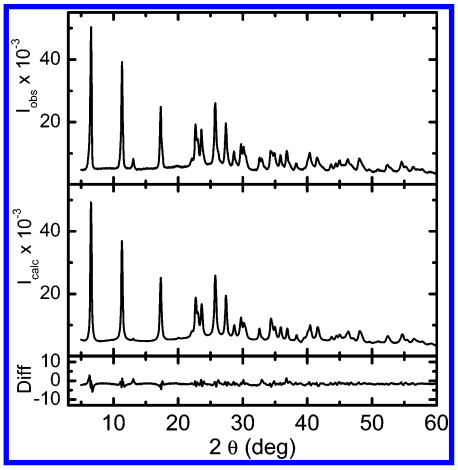

Figure 2. Experimental and calculated X-ray powder pattern for **2** (R_1 = Me, R_2 = Ph).

(20) Antonello, S.; Benassi, R.; Gavioli, G.; Tadei, F.; Maran, F. *J. Am. Chem. Soc.* **2002**, *124*, 7529.
(21) Barclay, T. M.; Cordes, A. W.; Goddard, J. D.; Mawhinney, R. C.; Oakley, R. T.; Preuss, K. E.; Reed, R. W. *J. Am. Chem. Soc.* **1997**, *119*, 12136.

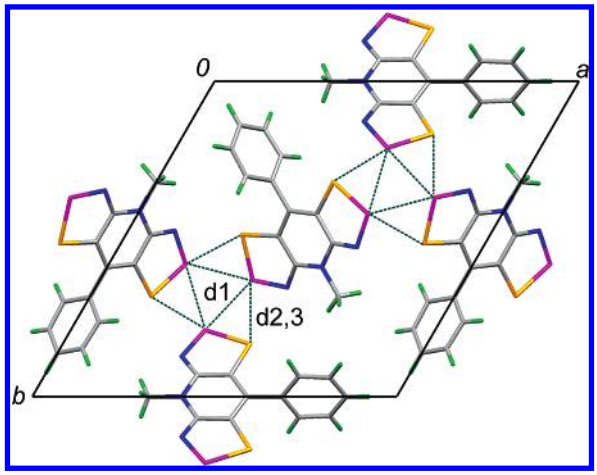

Figure 3. Unit-cell drawing of **2** (R_1 = Me, R_2 = Ph). Intermolecular contacts d1−d3 are defined in Table 3. (Color code: Se, pink; S, yellow; N, blue.)

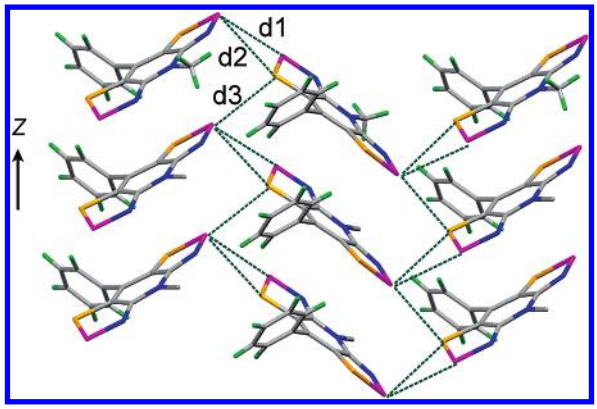

Figure 4. Herringbone π-stacking of **2** (R_1 = Me, R_2 = Ph). Intermolecular contacts d1−d3 are defined in Table 3. (Color code: Se, pink; S, yellow; N, blue.)

Table 3. Intermolecular S−S′, Se−S′, and Se−Se′ Contacts and Dihedral Angles

	1[a]		**2**[a]	
	(R_1 = Et)	(R_1 = Me)	(R_1 = Et)	(R_1 = Me)
d1 (Å)	3.430(3)	3.287(1)	3.397(2) [b]	3.34420(1) [b]
d2 (Å)	3.579(3)	3.507(1)	3.673(2)	3.6532(3)
d3 (Å)	3.407(3)	3.467(1)	3.595(3)	3.5002(2)
d4 (Å)	3.410(3)			
d5 (Å)	3.413(3)			
ϕ (deg)	6.6[c]	12.1	12.5	12.1

[a] R_2 = Ph for both **1** and **2**. [b] These are Se−Se′ contacts; the others listed for this molecule are Se−S′ contacts. [c] This is an average value from the four radicals in the asymmetric unit: range = 3.5−10.1°.

π-SOMOs,[22] in the lateral σ-fashion $[\mathbf{2}]_2$ (R_1 = Me, Et; R_2 = H),[13] or even in mixed σ/π-modes.[23] As we had hoped at the outset of this work, the steric influence of the ligands, that is, the nesting effect of the methyl/ethyl (R_1) and phenyl (R_2) groups about the 3-fold screw axis, produces a pinwheel-like clustering of the radicals (Figure 3) which militates against the lateral approach of the radicals and consequent formation of a σ-bonded dimer $[\mathbf{2}]_2$. In all three trigonal structures, the tricyclic framework of the radicals is not planar. There is a slight ruffling of the terminal five-membered rings to produce a propeller-like distortion about the 2-fold axis on which the molecules are located. Values of the dihedral angle ϕ between the two terminal rings are listed in Table 3. Viewed from the side, the π-stacks are locked into herringbone arrays (Figure 4) interconnected by a series of close intermolecular chalcogen−chalcogen contacts, d1−d3 (defined in Table 3), that lace the radical termini together about the 3-fold screw axis. All of these distances are well within the expected van der Waals separations for S−S′, S−Se′, and Se−Se′ contacts.[24] In addition, the contacts found in **2** (R_1 = Me, R_2 = Ph) are significantly shorter than those seen in **2** (R_1 = Et, R_2 = Ph). Collectively, they lead to a well-developed two-dimensional network of lattice-wide interactions transverse to the stacking direction.

In contrast to the structural similarity of the previous three radicals, replacement of the methyl group of **1** (R_1 = Me, R_2 = Ph) by an ethyl group to give **1** (R_1 = Et, R_2 = Ph), leads to a major structural reorganization. Crystals of the latter belong to the triclinic space group $P\bar{1}$ with $Z = 8$, that is, there are four radicals in the asymmetric unit (Figure 5). Individually, the radicals are still ruffled into a propellerlike conformation, although the average dihedral angle ϕ is smaller than that in the trigonal structures. The radicals also adopt a slipped π-stack motif, but now there are two distinct π-stacks (Figure 6). Moreover, within each of these stacks the phenyl rings pack in a tilted-T orientation[25] rather than a cofacial π-stacking pattern. This leads to a doubling of the cell dimension along the stack, although the radicals are not dimerized. Overall the packing of the radicals is much looser than in **1** (R_1 = Me, R_2 = Ph), a conclusion further substantiated by comparison of the two densities (1.649 g cm^{-1} for R_1 = Me vs 1.590 g cm^{-1} for R_1 = Et). Nonetheless, there remains a series of intermolecular S−S′ contacts (d1−d5) that lace the radicals into chains along the *y* direction, but they are longer and more localized interactions than those observed in **1** (R_1 = Me, R_2 = Ph). There are no close intermolecular S−S′ contacts in the *z* direction because the interpenetrating ethyl and phenyl groups serve to keep the radicals well separated.

Band Structures. In order to compare the extent of intermolecular electronic interactions in the three isostructural radicals **1** (R_1 = Me, R_2 = Ph) and **2** (R_1 = Me, Et; R_2 = Ph), we have performed a series of EHT band-structure calculations. The results are summarized in Figure 7, which shows the dispersion of the crystal orbitals (COs) resulting from the three SOMOs in the respective unit cells, plotted from Γ (0, 0, 0) to Z (0, 0, $^1/_2$) of the reciprocal cell, a

(22) (a) Cordes, A. W.; Haddon, R. C.; Oakley, R. T.; Schneemeyer, L. F.; Waszczak, J. V.; Young, K. M.; Zimmerman, N. M. *J. Am. Chem. Soc.* **1991**, *113*, 582. (b) Andrews, M. P.; Cordes, A. W.; Douglass, D. C.; Fleming, R. M.; Glarum, S. H.; Haddon, R. C.; Marsh, P.; Oakley, R. T.; Palstra, T. T. M.; Schneemeyer, L. F.; Trucks, G. W.; Tycko, R. R.; Waszczak, J. V.; Young, K. M.; Zimmerman, N. M. *J. Am. Chem. Soc.* **1991**, *113*, 3559. (c) Cordes, A. W.; Haddon, R. C.; Hicks, R. G.; Oakley, R. T.; Palstra, T. T. M.; Schneemeyer, L. F.; Waszczak, J. V. *J. Am. Chem. Soc.* **1992**, *114*, 1729. (d) Beer, L.; Cordes, A. W.; Myles, D. J. T.; Oakley, R. T.; Taylor, N. J. *CrystEngChem* **2000**, *2*, 109.
(23) Feeder, N.; Less, R. J.; Rawson, J. M.; Oliete, P.; Palacio, F. *Chem. Commun.* **2000**, 2449.
(24) Bondi, A. *J. Phys. Chem.* **1964**, *68*, 441.
(25) (a) Paliwal, S.; Geib, S.; Wilcox, C. S. *J. Am. Chem. Soc.* **1994**, *116*, 4491. (b) Nishio, M. *CrystEngComm* **2004**, *6*, 130.

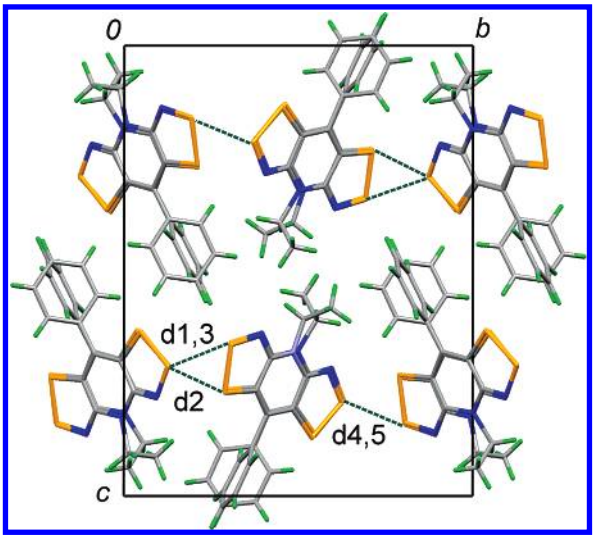

Figure 5. Unit-cell drawing of **1** (R_1 = Et, R_2 = Ph). Intermolecular contacts d1−d5 are defined in Table 3. (Color code: S, yellow; N, blue.)

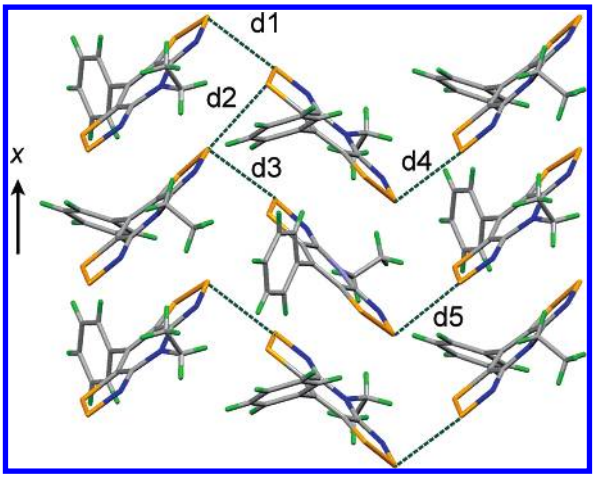

Figure 6. π-Stacking of **1** (R_1 = Et, R_2 = Ph). Intermolecular contacts d1−d5 are defined in Table 3. (Color code: S, yellow; N, blue.)

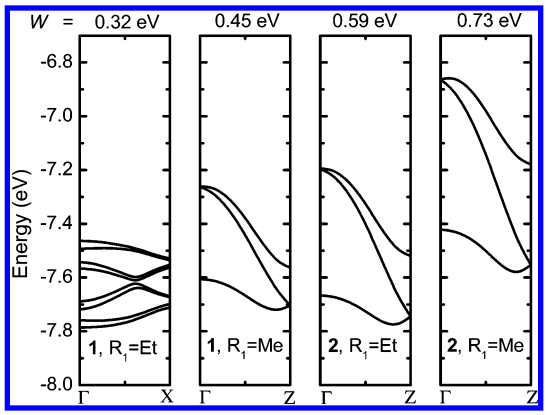

Figure 7. EHT band dispersion of SOMO-based crystal orbitals of **1** and **2** (R_1 = Me, Et; R_2 = Ph). The resultant bandwidths *W* are also shown.

direction which can be associated with the interactions along the stacking axis in real space. The dispersion curves of the eight COs originating from the SOMOs in the unit cell of **1** (R_1 = Et, R_2 = Ph) are also shown; this time, they are plotted from Γ (0, 0, 0) to X ($^1/_2$, 0, 0) of the reciprocal cell, a direction which corresponds loosely to the real space interaction along the stacking axis of the triclinic cell. The

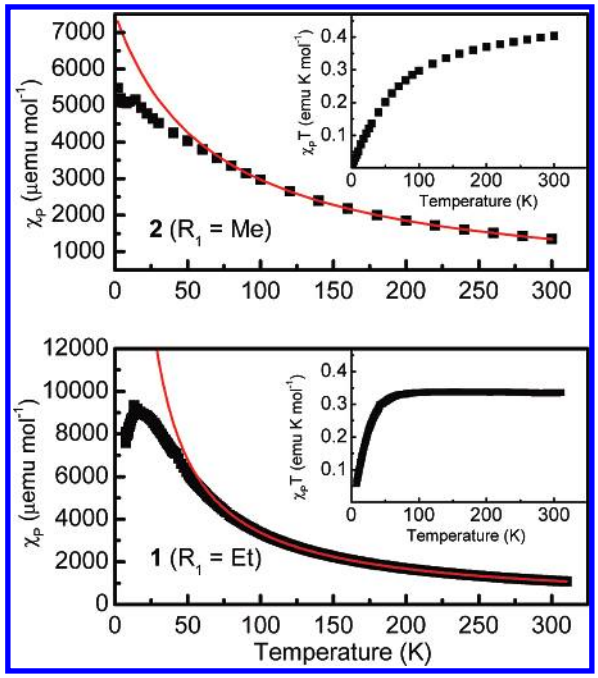

Figure 8. Plots of χ_P and $\chi_P T$ vs temperature (inset) for **1** (R_1 = Et, R_2 = Ph) and **2** (R_1 = Me, R_2 = Ph). Curie−Weiss fits to the high-temperature data are also shown.

bandwidths *W* estimated in terms of the energetic spread of the crystal orbitals over the range of reciprocal space under consideration are also shown.

Inspection of the degree of band spreading in the four compounds indicates that electronic interactions are weakest in **1** (R_1 = Et, R_2 = Ph) with W = 0.32 eV. This can be attributed to the less-efficient stacking of the radicals occasioned by the tilted-T packing of the phenyl rings, which doubles the cell repeat. Indeed, by virtue of the latter effect, a very small energy gap is opened at the Fermi level. The three isostructural radicals **1** and **2** (R_1 = Me, Et; R_2 = Ph) all show better band dispersion and, within the series, the trend can be easily rationalized. First, there is an increase in *W* from **1** and **2** (R_1 = Me, R_2 = Ph) of ∼60%, that is, replacement of sulfur by selenium has the desired effect, the heavier chalcogen affords stronger intermolecular overlap and hence increased bandwidth. Second, the difference in bandwidth between the two selenium-based radicals demonstrates the detrimental effect of steric bulk of the organic ligands, that is, their ability to keep the interacting radicals apart. In this instance, the replacement of a methyl group by an ethyl group leads to a 20% decrease in bandwidth.

Magnetic Susceptibility and Conductivity. Magnetic susceptibility measurements as a function of temperature have been performed on **1** and **2** (R_1 = Me, Et; R_2 = Ph). Figure 8 provides plots of χ_P (the susceptibility after correction for diamagnetic contributions χ_D)[26] and the product $\chi_P T$ for compounds **1** (R_1 = Et, R_2 = Ph), the structurally unique material and **2** (R_1 = Me, R_2 = Ph), which is representative of the three trigonal structures. The temperature dependence of χ_P for all four materials is consistent

(26) Estimated from Pascal's constants, see: Carlin, R. L. *Magnetochemistry*; Springer-Verlag: New York, 1986.

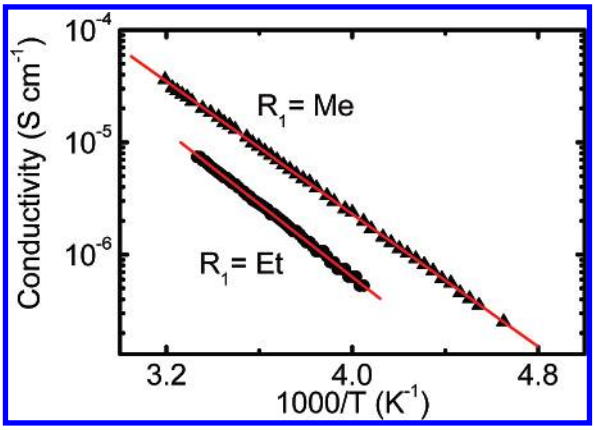

Figure 9. Conductivity of **2** (R_1 = Me, Et; R_2 = Ph) as a function of inverse temperature.

with essentially paramagnetic behavior above 100 K. The results of Curie Weiss fits to the high-temperature data are summarized in Table 1. At lower temperatures, there are minor deviations which are consistent with the onset of antiferromagnetic (AFM) exchange interactions. The degree of AFM coupling, measured in terms of the value of Θ, is variable within the isostructural trigonal series, but it is weakest in the double π-stack structure **1** (R_1 = Et, R_2 = Ph).

Preliminary two-probe pressed-pellet conductivity measurements on the two sulfur-containing compounds **1** (R_1 = Me, Et; R_2 = Ph) indicated room-temperature conductivities, σ_{RT}, of $\sim 10^{-7}$ S cm^{-1} for R_1 = Me and $<10^{-7}$ S cm^{-1} for R_1 = Et. More-detailed four-probe variable-temperature measurements were carried out on the two selenium-containing radicals **2** (R_1 = Me, Et; R_2 = Ph), the results of which are illustrated graphically in Figure 9. The ambient temperature conductivities σ(300 K) of the two compounds are 7.4×10^{-6} S cm^{-1} for R_1 = Et and 3.3×10^{-5} S cm^{-1} for R_1 = Me, indicative of the beneficial effect of selenium incorporation. In addition, while the conductivities remain activated, there is a marked decrease in the thermal activation energies, E_{act} = 0.32 (R_1 = Et) and 0.29 eV (R_1 = Me), relative to those of sulfur-based radicals **1**.

An internal comparison of the performance of the two selenium-based radicals reveals a trend heralded in the band calculations described above. The methyl derivative, with its more compact structure and higher electronic bandwidth, displays a higher conductivity and lower activation energy than the ethyl compound, a conclusion that underscores the importance of packing efficiency and close intermolecular interactions on conductivity. In an earlier communication,[15] we showed that the application of physical pressure (5 GPa) on **2** (R_1 = Et, R_2 = Ph) led to an increase in conductivity of $\sim$3 orders of magnitude. The present results illustrate that replacement of the ethyl group by a methyl group effects a smaller improvement, which may be attributed to the effect of "chemical pressure", that is, a more-efficient packing occasioned by the removal of steric constraints.

Summary and Conclusion. For some time, we have sought to generate isostructural thiazyl and selenazyl radicals, with a view to exploring the effect of the incorporation of the heavier chalcogen on bandwidth and conductivity. However, the propensity of selenium-containing radicals to associate with the formation of strong Se−Se σ-bonds has, to date, precluded any attempt to make such comparisons. In the present paper, we have described a simple one-step procedure for the regiospecific insertion of selenium into the two 2-positions of the bisdithiazolylium cations $[\mathbf{1}]^+$, to afford the corresponding selenium-containing materials $[\mathbf{2}]^+$. The packing of the subsequent radicals, **1** and **2**, and even their tendency to associate in the solid state is influenced by the size and shape of the R_1 and R_2 substituents. By using the sterically bulky phenyl group in the R_2 position we have been able, for the first time, to suppress dimerization of a selenazyl radical. Three of the four members of the family of radicals **1** and **2** (R_1 = Me, Et; R_2 = Ph) are isostructural, belonging to the space groups $P3_121$ or $P3_221$. Comparison of the EHT band structures of these related systems confirms that intermolecular interactions, and hence bandwidth and conductivity, are enhanced by the incorporation of selenium and the use of small R_1 groups (R_1 = Me vs Et). We are currently exploring the use of other combinations of (smaller) R_1 and R_2 ligands that will allow the crystallization of undimerized radicals, while at the same time providing for a greater degree of CO dispersion. Synthetic routes to allow the complete replacement of sulfur by selenium are also being pursued.

Experimental Section

General Procedures and Starting Materials. The reagents sulfur monochloride, selenium dioxide, methyl and ethyl triflate (trifluoromethanesulfonate), and decamethyl- and octamethylferrocene (DMFc and OMFc) were obtained commercially and used as received. Ammonia gas (reagent grade, Matheson) was also used as received. 2,6-Dichloro-4-phenyl-pyridine, **3**, was prepared by the chlorination of 2,6-dihydroxy-4-phenylpyridine,[27] and [**1**][OTf] (R_1 = Me, R_2 = Ph) was prepared as previously described.[10] All solvents were of at least reagent grade; acetonitrile (MeCN), dichloromethane (DCM), and dichloroethane (DCE) were dried by distillation from P_2O_5, CaH_2, or both. All reactions were performed under an atmosphere of dry nitrogen. Melting points are uncorrected. Infrared spectra (Nujol mulls, KBr optics) were recorded on a Nicolet Avatar FTIR spectrometer (at 2 cm^{-1} resolution), and ^{1}H NMR spectra were run on a Bruker Avance 300 MHz NMR spectrometer. Low-resolution mass spectra (70 eV, EI and ESI) were run on a Micromass Q-TOF Ultima Global LC/MS/MS system or a JEOL HX110 double-focusing mass spectrometer. Elemental analyses were performed by MHW Laboratories, Phoenix, AZ.

Preparation of 8-Phenyl-4-methyl-4*H*-bis[1,2,3]thiaselenazolo-[4,5-b:5′,4′-e]pyridin-2-ium Triflate [2][OTf] (R_1 = Me, R_2 = Ph). A slurry of [**1**][OTf] (R_1 = Me, R_2 = Ph) (1.03 g, 2.18 mmol) and selenium dioxide (0.756 g, 6.81 mmol) in 40 mL of HOAc and $\sim$2 mL of ethanol was brought to reflux. After 2 h, the reaction mixture was cooled to room temperature, and the resulting microcrystals of [**2**][OTf] (R_1 = Me, R_2 = Ph) were collected by suction filtration, washed with 3 × 50 mL of DCE, and dried in air. Yield: 1.02 g (1.80 mmol, 83%). Recrystallization from MeCN

(27) (a) Balicki, R.; Kaczmarek, L.; Nanyka-Namirski, P. *Pol. J. Chem.* **1979**, *53*, 2491. (b) Kambe, S.; Saito, K.; Sakurai, A.; Hayashi, T. *Synthesis* **1977**, 841. (c) Al-Jallo, H. N.; Al-Biaty, A.; Al-Azawi, F. N. *J. Heterocyclic Chem.* **1977**, *14*, 1347.

yielded red crystalline blocks. mp: 285−287 °C. IR: ν' 1498 (w), 1407 (m), 1344 (w), 1239 (s) 1200 (vw), 1162 (w), 1046 (vw), 1021 (vs), 956 (vw), 850 (vw), 790 (w), 761 (w), 727 (vs), 655 (m), 635 (vs), 603 (s), 573 (w), 538 (w), 513 (vs), 455 (s) cm^{-1}. ^1H NMR (CD_3CN): δ 7.68−7.50 (m, 5H), 3.74 (s, 3H). Anal. Calcd for $C_{13}H_8F_3N_3O_3S_3Se_2$: C, 27.62; H, 1.43; N, 7.43%. Found: C, 27.69; H, 1.52; N, 7.44%.

Preparation of 8-Phenyl-4-methyl-4*H*-bis[1,2,3]thiaselenazolo-[4,5-b:5′,4′-e]pyridinyl 2 (R_1 = Me, R_2 = Ph). Degassed solutions (3 freeze−pump−thaw cycles) of DMFc (121 mg, 0.371 mmol) in MeCN (80 mL) and [**2**][OTf] (R_1 = Me, R_2 = Ph) (200 mg, 0.354 mmol) in MeCN (100 mL) were combined and stirred at room temperature for 1 h. Copper-colored microcrystalline needles of **2** (R_1 = Me, R_2 = Ph) were separated by filtration and dried in vacuo. Yield: 125 mg (0.30 mmol, 85%). IR: ν' 1241 (vs), 1179 (s), 1075 (w), 1038 (s), 999 (w), 948 (w), 916 (w), 864 (w), 816 (s), 779 (m), 725 (vs), 702 (vs), 646 (s), 623 (w), 589 (m), 578 (m), 536 (m), 502 (w), 438 (s) cm^{-1}.

Preparation of *N*-Ethyl-2,6-dichloro-4-phenyl-pyridinium Triflate 4 (R_1 = Et, R_2 = Ph). Ethyl triflate (5.0 g, 28.1 mmol) was added to a solution of 2,6-dichloro-4-phenylpyridine **3** (5.23 g, 23.3 mmol) in 60 mL of DCE. The reaction mixture was stirred for 16 h at reflux and cooled to −20 °C, and the white precipitate was collected by filtration, washed with cold diethyl ether, and dried in vacuo. Yield: 8.95 g (22.3 mmol, 95%). Recrystallization from hot DCE yielded analytically pure **4** (R_1 = Et, R_2 = Ph). mp: 140−143 °C. IR: ν' 3083 (w), 3037 (vw), 1610 (vs), 1595 (m), 1534 (m), 1481 (w), 1409 (w), 1277 (vs), 1256 (vs), 1224 (m), 1152 (s), 1128 (m), 1090 (w), 1033 (vs), 893 (m), 840 (m), 778 (s), 692 (m), 641 (vs), 574 (m), 517 (s) cm^{-1}. ^1H NMR (CD_3CN): δ 8.37 (s, 2H), 7.93−7.95 and 7.62−7.71 (m, 5H), 4.93 (q, 2H), 1.56 (t, 3H). Anal. Calcd for $C_{14}H_{12}Cl_2F_3NO_3S$: C, 41.81; H, 3.01; N, 3.48%. Found: C, 41.67; H, 3.26; N, 3.31%.

Preparation of *N*-Ethyl-2,6-diamino-4-phenyl-pyridinium Triflate 5 (R_1 = Et, R_2 = Ph). A solution of **4** (R_1 = Et, R_2 = Ph) (13.2 g, 32.8 mmol) in 120 mL of MeCN was cooled to 0 °C and saturated with anhydrous ammonia gas. A white precipitate formed immediately, and the solution became yellow. The mixture was sealed in a glass pressure reactor and heated, with stirring, to 85 °C. After 16 h, the vessel was cooled to room temperature and vented. The mixture was heated to reflux for an additional 2 h to release excess ammonia and cooled to room temperature, and the white precipitate was filtered off. The filtrate was concentrated to dryness, and the product **5** (R_1 = Et, R_2 = Ph) recrystallized from MeCN. Yield: 10.5 g (28.9 mmol, 88%). mp: 188−192 °C. IR: ν' 3453 (m), 3362 (s), 3248 (s), 1640 (vs), 1587 (m), 1566 (vs), 1490 (m), 1332 (m), 1272 (vs), 1252 (vs), 1226 (m), 1173 (s), 1158 (s), 1031 (vs), 969 (w), 842 (w), 823 (w), 768 (s), 760 (m), 697 (m), 640 (vs), 576 (m), 517 (s), 475 (w) cm^{-1}. ^1H NMR (CD_3CN): δ 7.66−7.50 (m, 5H), 6.46 (s, 2H), 6.17 (s, 4H), 3.98 (q, 2H), 1.36 (t, 3H). Anal. Calcd for $C_{14}H_{16}F_3N_3O_3S$: C, 46.28; H, 4.44; N, 11.56%. Found: C, 46.40; H, 4.16; N, 11.37%.

Preparation of 8-Phenyl-4-ethyl-4*H*-bis[1,2,3]dithiazolo[4,5-b:5′,4′-e]pyridin-2-ium Triflate [1][OTf] (R_1 = Et, R_2 = Ph). Sulfur monochloride (28.7 g, 0.213 mol) was added to a stirred solution of **5** (R_1 = Et, R_2 = Ph) (5.56 g, 15.3 mmol) in 50 mL of a 1:20 (v/v) mixture of MeCN/DCE. The initially green solution was heated at gentle reflux for 16 h to afford a deep blue solution and a red precipitate. The mixture was cooled to 0 °C, and the product, [**1**][OTf] (R_1 = Et, R_2 = Ph), was filtered off, washed with 3 × 75 mL of DCE, and dried in vacuo. Yield: 6.61 g (13.6 mmol, 89%). Recrystallization from hot MeCN yielded lustrous red plates. mp: 288−290 °C. IR: ν' 1524 (w), 1508 (w), 1424 (s), 1364 (s), 1271 (s), 1242 (s), 1223 (m), 1189 (m), 1061 (s), 1084 (m), 1027 (s), 891 (w), 820 (m), 790 (s), 746 (s), 730 (s), 668 (s), 637 (s), 601 (w), 566 (w), 516 (w), 484 (s) cm^{-1}. ^1H NMR (CD_3CN): δ 7.70−7.55 (m, 5H), 4.20 (q, 2H), 1.33 (t, 3H). Anal. Calcd for $C_{14}H_{10}F_3N_3O_3S_5$: C, 34.63; H, 2.08; N, 8.65%. Found: C, 34.86; H, 2.21; N, 8.71%.

Preparation of 8-Phenyl-4-ethyl-4*H*-bis[1,2,3]thiaselenazolo-[4,5-b:5′,4′-e]pyridin-2-ium Triflate[2][OTf] (R_1 = Et, R_2 = Ph). A stirred slurry of [**1**][OTf] (R_1 = Et, R_2 = Ph) (1.00 g, 2.06 mmol) and selenium dioxide (0.686 g, 6.18 mmol) in 20 mL of HOAc and ∼1 mL of ethanol was brought to reflux. After 2 h, the reaction mixture was cooled to room temperature, and the resulting microcrystals of [**2**][OTf] (R_1 = Et, R_2 = Ph) were collected by suction filtration, washed with 3 × 50 mL of DCE, and dried in air. Yield: 1.14 g (1.97 mmol, 96%). Recrystallization from MeCN/DCE yielded red crystals. mp: 284−286 °C. IR: ν' 1492 (vw), 1424 (s), 1270 (m), 1243 (s), 1223 (m), 1185 (w), 1156 (m), 1073 (w), 1027 (vs), 864 (vw), 756 (vw), 730 (vs), 701 (m), 654 (m), 638 (vs), 596 (vs), 519 (m), 513 (m), 455 (m) cm^{-1}. ^1H NMR (CD_3CN): δ 7.70−7.50 (m, 5H), 4.31 (q, 2H), 1.34 (t, 3H). Anal. Calcd for $C_{13}H_8F_3N_3O_3S_3Se_2$: C, 29.02; H, 1.74; N, 7.25%. Found: C, 29.22; H, 1.82; N, 7.32%.

Preparation of 8-Phenyl-4-ethyl-4H-bis[1,2,3]dithiazolo[4,5-b:5′,4′-e]pyridinyl 1 (R_1 = Et, R_2 = Ph). Degassed solutions (3 freeze−pump−thaw cycles) of DMFc (20 mg, 0.06 mmol) in 15 mL of MeCN and [**1**][OTf] (R_1 = Et, R_2 = Ph) (25 mg, 0.07 mmol) in 5 mL of MeCN were allowed to diffuse together slowly at room temperature over a period of 16 h. The solvent was decanted to leave metallic green crystals. mp: 179−182 °C. IR: ν' 1534 (vw), 1507 (vw), 1296 (vw), 1200 (vs), 1177 (m), 1077 (m), 1070 (m), 1027 (w), 1001 (m), 920 (m), 868 (m), 792 (s), 779 (m), 735 (vs), 704 (vs), 662 (s), 655 (s), 645 (m), 621 (vw), 590 (s), 561 (s), 539 (vw), 491 (w), 471 (m), 463 (s) cm^{-1}. Anal. Calcd for $C_{13}H_{10}N_3S_4$: C, 46.40; H, 3.00; N, 12.49%. Found: C, 46.61; H, 3.08; N, 12.49%.

Preparation of 8-Phenyl-4-ethyl-4*H*-bis[1,2,3]thiaselenazolo-[4,5-b:5′,4′-e]pyridinyl 2 (R_1 = Et, R_2 = Ph). Degassed solutions (3 freeze−pump−thaw cycles) of OMFc (26 mg, 0.087 mmol) in MeCN (15 mL) and [**2**][OTf] (R_1 = Et, R_2 = Ph) (25 mg, 0.043 mmol) in MeCN (8 mL) were allowed to diffuse together slowly at 0 °C over a period of 16 h. The solvent was decanted to leave metallic green crystals of **2** (R_1 = Et, R_2 = Ph). mp: 170−173 °C. IR: ν' 1441 (s), 1403 (vw), 1364 (w), 1344 (vw), 1299 (w), 1214 (s), 1171 (vw), 1066 (w), 832 (w), 720 (m), 707 (s), 648 (w), 594 (w), 436 (w) cm^{-1}.

Single-Crystal X-ray Diffraction. Needles of **1** (R_1 = Et, R_2 = Ph) were glued to a glass fiber with epoxy. X-ray data were collected on a Bruker SMART APEX CCD-based diffractometer using ω-scans. The reflection data were processed using SAINT.[28] The structure was solved by direct methods using SHELXS-90[29] and refined by least-squares methods on F^2 using SHELXL-97[30] incorporated in the SHELXTL[31] suite of programs. The structure was refined in $P\bar{1}$ and contained 4 independent molecules in the asymmetric unit. It was suggested by XPREP that the cell could be converted to a C-centered metrically monoclinic cell; however, there was no evidence of 2-fold or mirror symmetry in the packing.

(28) *SAINT*, version 6.22; Bruker Advanced X-ray Solutions, Inc.: Madison, WI, 2001.
(29) Sheldrick, G. M. SHELXS-90. *Acta Crystallogr. A* **1990**, *46*, 467.
(30) Sheldrick, G. M. *SHELXL-97, Program for the Refinement of Crystal Structures*; University of Göttingen: Göttingen, Germany, 1997.
(31) *SHELXTL*, version 6.12; Bruker Advanced X-ray Solutions, Inc.: Madison, WI, 2001.

Furthermore, higher symmetry would induce disorder, whereas the triclinic cell was completely ordered. The pseudomonoclinic metrics did allow for the observed twinning and thus was included in the refinement. The subroutine addsym[32] of the PLATON package[33] was employed to look for higher symmetry, in particular for monoclinic C-centering. As expected, in addition to the inversion center, no symmetry element was found to exist. Therefore the space group $P\bar{1}$ was selected as the final space group for our model. All non-hydrogen atoms were refined anisotropically; hydrogen atoms were located on difference maps and refined isotropically. Details of data collection and refinement are presented in Table 2.

Powder X-ray Diffraction. A powdered sample (~60 mg) of **2** (R_1 = Me, R_2 = Ph) was loaded into an aluminum sample holder which was rotated during data collection. The diffraction pattern was collected at ambient temperature on a X-ray powder diffractometer with a position sensitive detector (INEL) using Cu $K\alpha_1$ radiation (λ = 1.54056 Å). The total 2θ range was 0.28−112.684°, measured in steps of 0.029° over a period of 3 h. The powder diffraction pattern was indexed by the program Taup[34] to give the following trigonal cell: a = 15.6837 Å, c = 4.6811 Å. When these data were compared to the unit-cell parameters for **1** (R_1 = Me, R_2 = Ph) and **2** (R_1 = Et, R_2 = Ph), it was evident that the three compounds were isostructural (save for chirality), and the space group $P3_121$ was arbitrarily selected. Starting with the coordinates for **1** (R_1 = Me, R_2 = Ph) as the initial model, we refined the structure by Rietveld methods[35] using the GSAS program package.[36] Data were refined from 5.0 to 60.0°, and all atoms, including hydrogens, were used in the refinement. Isotropic displacement parameters were refined for all non-hydrogen atoms, excluding ligand (Me and Ph) carbons, which were assigned a value of 0.025. The final Rietveld refinement gave agreement indices wR_p = 7.79% and R_p = 5.73%.

EPR Spectra. The X-Band EPR spectra were recorded at ambient temperature using a Bruker EMX-200 spectrometer on samples dissolved in degassed dichloromethane. Hyperfine coupling constants were obtained by spectral simulation using Simfonia.[37]

Band-Structure Calculations. Electronic band-structure calculations were performed with the EHMACC suite of programs[38] using the Coulomb parameters of Baasch, Viste, and Gray[39] and a quasisplit valence basis set adapted from Clementi and Roetti;[40] numerical values are tabulated elsewhere.[22a] The off-diagonal elements of the Hamiltonian matrix were calculated with the standard weighting formula.[41] Atomic positions were taken from the crystallographic data.

Magnetic Susceptibility Measurements. Magnetic susceptibility measurements on **1** (R_1 = Et, R_2 = Ph) were performed over the temperature range of 7−310 K on a George Associates Faraday balance operating at 0.5 T. Measurements on **2** (R_1 = Me, R_2 = Ph) were collected over the range of 2−300 K using a Quantum Design MPMS5S Squid magnetometer operating at 0.1 T.

Conductivity Measurements. Temperature-dependent conductivity measurements were performed on pressed pellet samples of **2** (R_1 = Me, Et; R_2 = Ph) using a four-probe method. A homemade device was used to measure the voltage drop under dynamic vacuum. Silver paint was used to apply the electrical contacts.

Acknowledgment. We thank the Natural Sciences and Engineering Research Council of Canada (NSERCC) and the U.S. Office of Basic Energy Sciences, Department of Energy (Grant DEFG02-04ER46138) for financial support. We also thank the Kentucky Research Challenge Trust Fund for the purchase of CCD X-ray equipment and an X-ray facility upgrade, the Ontario Provincial Government for a postgraduate scholarship to J.L.B., and the Canada Council for the Arts for a Killam Research Fellowship to R.T.O.

Supporting Information Available: Details of X-ray crystallographic data collection and structure refinement, tables of atomic coordinates, bond distances and angles, anisotropic thermal parameters, and hydrogen atom positions in CIF format. This material is available free of charge via the Internet at http://pubs.acs.org.

IC061687C

(32) Page, Y. L. *J. Appl. Crystallogr.* **1988**, *21*, 983.
(33) Spek, A. L. *J. Appl. Crystallogr.* **2003**, *36*, 7.
(34) Taupin, D. G. *J. Appl. Crystallogr.* **1969**, *2*, 179.
(35) Rietveld, H. M. *J. Appl. Crystallogr.* **1969**, *2*, 65.
(36) Larson, A. C.; Von Dreele, R. B. Report LA-UR-86-748; Los Alamos National Laboratory: Los Alamos, NM, 1987.
(37) *WinEPR Simfonia*; Bruker Instruments, Inc.: Billerica, MA.
(38) EHMACC, Quantum Chemistry Program Exchange, program number 571.
(39) Basch, H.; Viste, A.; Gray, H. B. *Theor. Chim. Acta* **1965**, *3*, 458.
(40) Clementi, E.; Roetti, C. *At. Data. Nucl. Data Tables* **1974**, *14*, 177.
(41) Ammeter, J. H.; Bürgi, H. B.; Thibeault, J. C.; Hoffmann, R. *J. Am. Chem. Soc.* **1978**, *100*, 3686.